Volumetric Recombination in the Linear ECR Plasma Device NUMBER*)

Konan YAGASAKI, Atsushi OKAMOTO, Takaaki FUJITA, Minami SUGIMOTO, Shunya HIGUCHI, Muneo KOIKE, Koki SATO and Yuto YAMADA

Nagoya University, Nagoya 464-8603, Japan

(Received 9 January 2023 / Accepted 26 June 2023)

A plasma recombination experiment was carried out using the linear electron cyclotron resonance (ECR) plasma device NUMBER as a preliminary step for forming a detached plasma. The electron density measured by an electrostatic probe in a divertor-simulated region was successfully increased up to approximately 6×10^{17} m^{-3}. This increase was realized by installing an additional gas feed system to the region and using a circular polarizer to control the microwave polarization. Passive spectroscopic measurements performed on the high-density plasma yielded line spectra of He I 2^3P–n^3D for the principal quantum number $n \leq 13$, which are characterstic of helium recombining plasma. The line spectra were used to calculate an electron temperature of approximately 0.055 eV and an electron density of approximately 1.33×10^{18} m^{-3} by the Boltzmann plot method and Saha–Boltzmann equation, respectively.

Keywords: recombining plasma, volumetric recombination, ECR plasma, polarization, electron density

DOI: 10.1585/pfr.18.2401082

1. Introduction

In tokamak fusion reactors, a plasma is eventually transported along magnetic field lines in the scrape-off layer (SOL) to a divertor. The steady-state heat flux into the DEMO divertor plate is expected to be more than 10 MW/m^2, even when radiation loss is sufficiently accounted for. However, the heat capacity of the divertor plate is considered to be below 10 MW/m^2 [1]. Thus, heat-load reduction strategies are being investigated to realize steady-state operation and extend the life of the divertor. The most promising of these strategies is inducing volumetric recombination to form a detached plasma in the divertor.

To elucidate the atomic processes that occur in an SOL–divertor plasma, extensive simulations on divertor plasma have been performed by utilizing linear plasma device. The simple configuration of these devices provides flexibility in the experiments [2]. These linear plasma devices utilize a variety of plasma sources, such as direct current arc discharge [3], radio frequency discharge [4], and electron cyclotron resonance (ECR). A linear plasma device used in this study, NUMBER [5], is employing an ECR plasma source. ECR is considered to be capable of producing nonequilibrium and anisotropic plasmas. These are considered to be a cause of uncertainty in the detachment physics.

However, we have not observed a detached plasma or a volumetric recombining plasma in the experiments using NUMBER. This result was obtained for two main reasons. The first reason is that the electron density of the plasma is a few orders of magnitude lower than that achieved in devices employing other plasma sources. A plasma with a high electron density n_e and a low electron temperature T_e is required to induce volumetric recombination. Two experimental parameters are known to increase the electron density n_e: the forward microwave power P_{for} and the neutral pressure p_n in the divertor-simulated region. However, the electron density has not been able to be increased sufficiently to induce volumetric recombination.

The second reason is the coexistence of different pressure requirements in the device. A relatively low pressure of below 1 Pa is required to produce a plasma by ECR. However, the neutral pressure in the divertor-simulated region should be near that of a real divertor, i.e., approximately 10 Pa. This difference in the two aforementioned pressure requirements may inhibit ECR plasma production or narrow the window of conditions over which a recombining plasma can be generated.

In this paper, improvements made to NUMBER to increase the electron density of the plasma and the results of plasma diagnostics are reported. The first observation of volumetric recombination is then presented. The experimental setup is described in Section 2. The implementation of the improvements are described in Section 3, and the results of plasma experiments are presented in Section 4. The study results are summarized in Section 5.

author's e-mail: k.yagasaki@kyotofusioneering.com

*) This article is based on the presentation at the 31st International Toki Conference on Plasma and Fusion Research (ITC31).

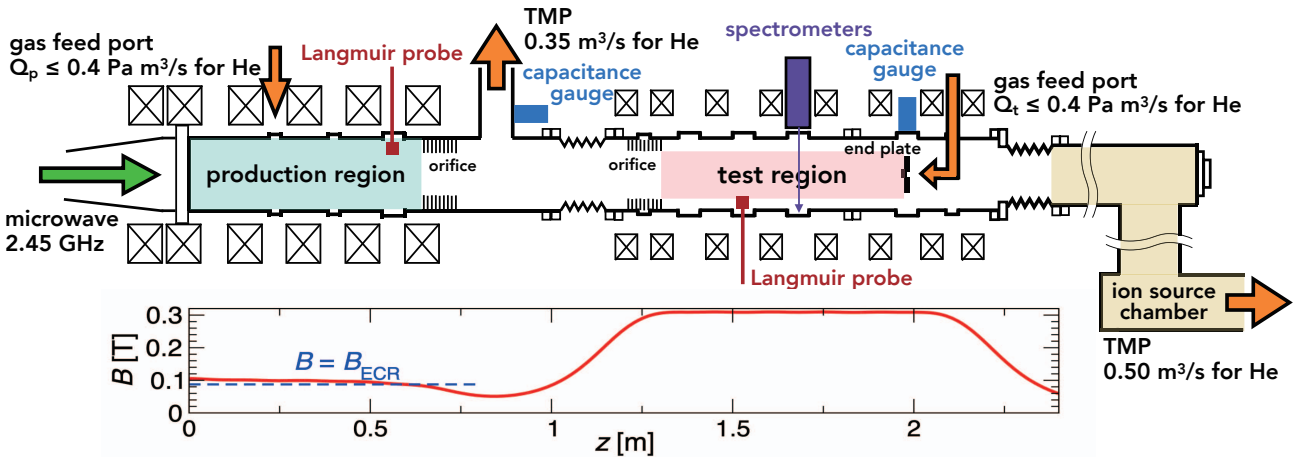

Fig. 1 A schematic of NUMBER and the magnetic field at the center of the cylindrical vacuum vessel at $t \sim 13$ ms.

2. Experimental Setup

NUMBER is a linear plasma device with a cylindrical vacuum vessel of 0.2 m diameter and 4 m length. Figure 1 shows the three regions in the device in which plasma experiments are carried out. In the production region, an overdense plasma is produced by ECR using a continuous microwave at 2.45 GHz under a steady-state ~ 0.1 T magnetic field. The microwave is injected along the magnetic field lines from the high-field side. The maximum incident power of the microwaves is 6 kW. The microwave is converted from the rectangular TE_{10} mode to the circular TE_{11} mode before being injected through a quartz window into the device. The plasma is transported from the production region to the test region (divertor-simulated region) by applying a magnetic field of $B_{test} \lesssim 0.3$ T to the test region, and is terminated by an end plate. In the production and test regions, the plasma is measured using electrostatic probes at $z = 0.57$ m and $z = 1.53$ m, and passive spectroscopic measurement at $z = 1.68$ m. An ion-source chamber is located behind the test region and utilized as an exhaust path in the present experiments. The typical plasma parameters for NUMBER in the test region are $n_e \sim 1$–2×10^{17} m^{-3} and $T_e \sim 5$ eV. The typical time dependences of these parameters are shown in Fig. 2.

Helium gas was initially fed only to the plasma production region at a constant flow rate $Q_p \leq 0.05$ Pa m^3/s. The gas was differentially exhausted using one or both of two turbo-molecular pumps. Experiments in this paper are carried out with exhaust by only one pump installed between the production and test regions except for the experiments described in Section 4.2, which uses two pumps. The neutral gas pressure was measured by two capacitance diaphragm gauges. One gauge was installed at the z position of the end plate [6], and the second gauge was installed between the two regions, at $z = 0.85$ m. The first gauge was used in the experiment except for the case shown in Fig. 7, which uses the two gauges. To feed a sufficient quantity of neutral gas into the device, a high-flow-rate mass flow controller (MFC) was installed in parallel with a low-flow-rate

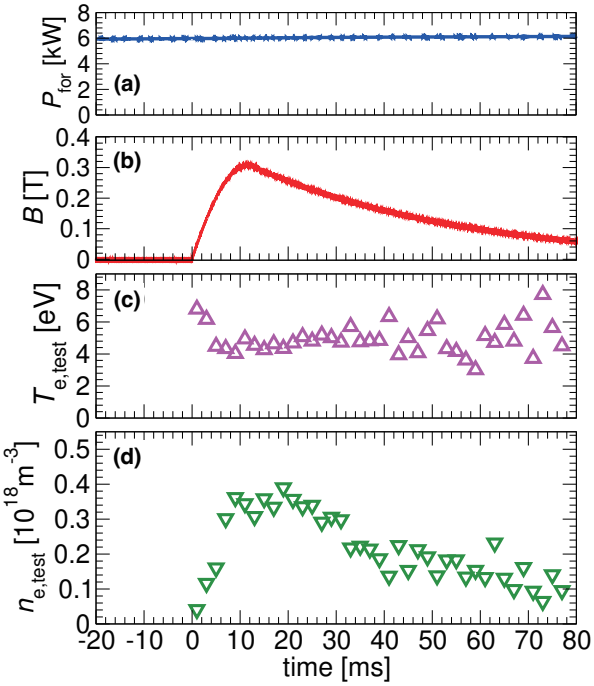

Fig. 2 Typical time dependence of (a) the forward microwave power P_{for}, (b) magnetic field in the test region B, (c) electron temperature in the test region $T_{e,test}$, and (d) electron density in the test region $n_{e,test}$.

MFC. The maximum flow rate of the high-flow-rate MFC is 0.85 Pa m^3/s, and gas can be fed up to 0.40 Pa m^3/s in practice. A new feed port was installed in the test region. The gas feed opening is located at the center of the cylindrical vacuum vessel and used to feed gas axisymmetrically from behind the end plate. Thus, NUMBER offers flexibility in using these different combinations of the two gas feeding ports and two mass flow controllers. This improvement enabled a pressure of 5 Pa to be achieved in the test region. This pressure is comparable to that expected for a DEMO divertor [7]. Higher pressures could be achieved by reducing the conductance of the gate valves at the front of the turbo-molecular pumps.

3. Installation of a Circular Polarizer

Increasing the forward microwave power caused an increase in n_e, which however was still not sufficient to generate recombining plasma, even at the maximum forward power. Therefore, we investigated varying the polarization state of the microwaves. The incident microwaves were linearly polarized, and approximately 60% of the forward power was reflected back without being absorbed by the plasma. We installed a Teflon circular polarizer in the waveguide (see Fig. 3) to induce a right-handed circular polarization in the microwave, such that the microwave could be effectively absorbed by the plasma as a R-wave [8]. The polarizer dimensions were based on those used in Noguchi *et al.* [9]. To prevent the polarizer from being damaged by excessive microwave irradiation, the microwave injection time is sequence-controlled to 1 second, which is the shortest reasonable injection time for conducting experiments. The polarizer is fixed in a 2 cm-long circular waveguide, as shown in Fig. 3, that is then inserted into the existing circular waveguide section. The polarizer can be rotated by 45 degrees for mounting.

An experiment was carried out on the installed polarizer to confirm its effectiveness. The experiment consisted of varying the mounting pattern of the polarizer, and measuring the forward and reflected microwave power (P_{for} and P_{ref}, respectively). The results are shown in Fig. 4. The mounting patterns are shown in Fig. 4 (c). Before the polarizer was installed, P_{ref}/P_{for} was ~ 60 % (Pattern 1).

Pattern 2 was corresponding to a 2-cm extension of the circular waveguide in the absence of a polarizer. Pattern 2 resulted in a slight decrease in the ratio of the reflected power to the forward power (the reflection ratio), which was attributed to a change in the wave transmission caused by the change in the waveguide length.

The polarization direction in Pattern 3 is that of the E field of the incident microwave. However, the reflection ratio decreased even when Pattern 3 was used, which was considered to result from the insertion of the dielectric being inserted into the waveguide. Pattern 4 is the configuration used to induce a right-handed circular polarization in the microwave. The reflected power reached a minimum for Pattern 4, as expected. That is, P_{ref}/P_{for} decreased to ~ 20 %. However, even under a pattern of inducing left-handed circular polarization (Pattern 6), P_{ref}/P_{for} decreased to ~ 20 %. The cause of the decrease in the reflection ratio is unknown. One possible explanation for this result is absorption induced by inversion of the polarization to the L-wave near the ECR point [10, 11].

The forward microwave power was varied for Pattern 4. The results are compared with those obtained before the polarizer was installed in Fig. 5. The installation of the circular polarizer resulted in a decrease of the reflected microwave power P_{ref} over the full range of the forward power (see Fig. 5 (a)). This result implies that a right-handed circular polarization was successfully induced by the polarizer. The polarizer caused the ion saturation current in the test region to increase (see Fig. 5 (b)), where the horizontal axis is the port-through input power P_{pt} defined as below:

$$P_{pt} = P_{for} - P_{ref}. \quad (1)$$

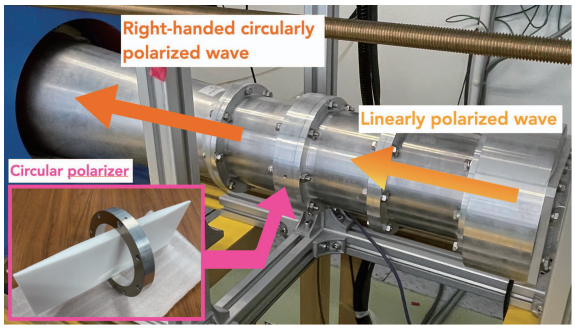

Fig. 3 Polarizer installation.

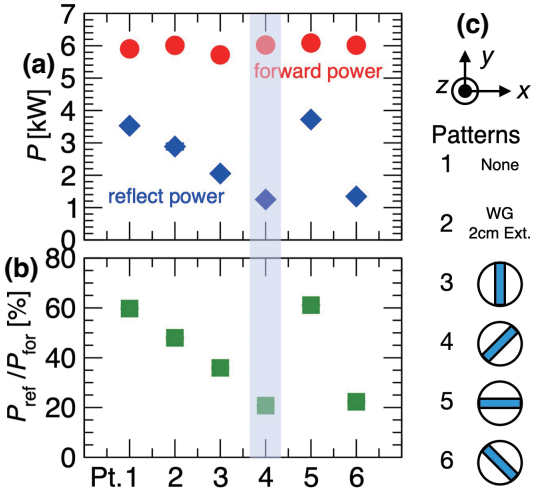

Fig. 4 (a) Forward and reflected power for each mounting patterns of the polarizer. (b) The ratio of the reflected power to the forward power. (c) Schematic of the mounting patterns.

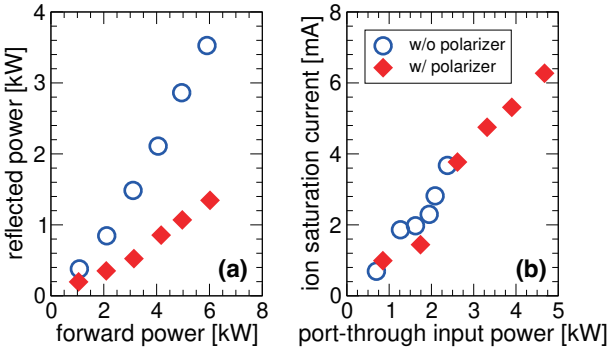

Fig. 5 (a) The reflected power as a function of the forward power and (b) the ion saturation current in the test region as a function of the port-through input power.

4. Results

4.1 Varying the experimental parameters

After the ion saturation current was measured (the results are shown in Fig. 5), an electrostatic probe was used to measure the electron temperature T_e and electron density n_e in the test region over a range of microwave powers (see Fig. 6). T_e was almost constant in the high power region at approximately 5 eV. By contrast, n_e increased monotonically. The gas flow rate $Q_p = 0.05\,\mathrm{Pa\,m^3/s}$ corresponded to the upper limit of the low-flow-rate MFC.

A high-flow-rate MFC was then installed to feed gas from the production region, and the dependence of T_e and n_e on the neutral pressure was confirmed. The gas flow rate was varied over the range of 0.05–0.40 $\mathrm{Pa\,m^3/s}$. The corresponding neutral pressure range was 0.3–2 Pa. The results are shown in Fig. 7. The circular polarizer caused n_e to increase in both the production and test regions. In the production region, $n_{e,prod}$ reached approximately $10^{18}\,\mathrm{m^{-3}}$ at the maximum. In the test region, $n_{e,test}$ was increased by a factor of two, where the highest value was approximately $0.6 \times 10^{18}\,\mathrm{m^{-3}}$. Since the rate coefficient of three-body recombination is proportional to n_e, these results imply that a good plasma that is capable of forming recombining plasma is produced in NUMBER. However, relatively little change was observed in T_e in both the production and test regions. It can be concluded that increasing the neutral pressure did not positively affect T_e.

Next, passive spectroscopy measurements were carried out on the high n_e plasma in the test region. In a helium plasma, volumetric recombination is characterized by the emission of HeI 2^3P–n^3D for the principal quantum number $n \geq 10$. Observation of these emissions is evidence of the generation of a recombining plasma. Figure 8 shows the measured results obtained using a 1200/mm diffraction grating over the wavelength range 342–378 mm, including the corresponding spectra.

In Fig. 8, the line spectra can be identified for $n \leq 8$, but are unclear for $n \geq 9$. Thus, a recombining plasma was not observed even under the experimental conditions where the highest n_e was obtained by controlling the flow rate from the production region Q_p.

4.2 Feeding additional gas into the test region

In order to generate recombining plasma, an experiment to feed additional gas to the test region via a newly installed port was carried out. The aim of this experiment was to directly feed neutral gas into the test region, thereby increasing n_e by ionization and decreasing T_e by collisions with the neutral gas. The flow rate to the production region Q_p was fixed at $0.05\,\mathrm{Pa\,m^3/s}$, and the flow rate to the test region Q_t was varied between 0.17 and $0.40\,\mathrm{Pa\,m^3/s}$.

The electrostatic probe measurements are shown in Fig. 9. The error bars in the figure represent the standard deviation in the data over a time range of $10 \leq t \leq 30$ ms,

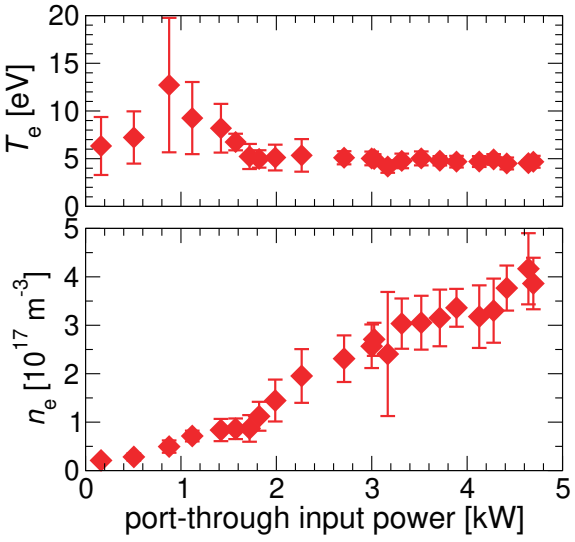

Fig. 6 Results obtained by varying P_{for}: T_e and n_e in the test region ($10 \leq t \leq 30$ ms, $P_{pt} = 4.7$ kW, $Q_p = 0.05\,\mathrm{Pa\,m^3/s}$, $Q_t = 0\,\mathrm{Pa\,m^3/s}$, $p_n = 0.32$ Pa).

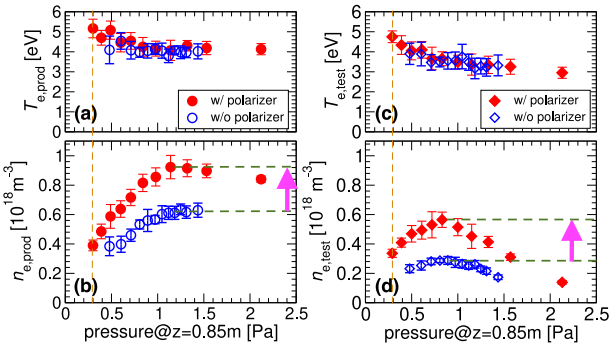

Fig. 7 Neutral pressure dependence of the (a) and (c) electron temperature and (b) and (d) electron density in the (a) and (b) production region and (c) and (d) test region ($10 \leq t \leq 30$ ms, $P_{pt} = 4.7$ kW). The vertical broken lines indicate the upper limit of the low-flow-rate MFC. The pressure was measured at $z = 0.85$ m.

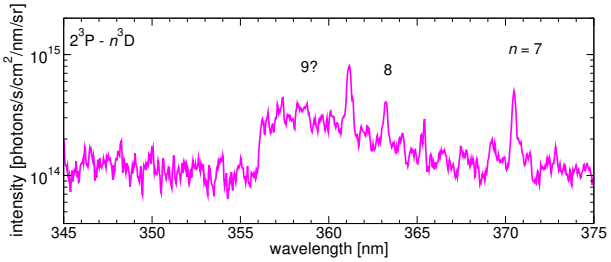

Fig. 8 Spectroscopic data of an He plasma with the highest n_e in the test region ($15 \leq t \leq 17$ ms, $P_{pt} = 4.7$ kW, $Q_p = 0.135\,\mathrm{Pa\,m^3/s}$, $Q_t = 0\,\mathrm{Pa\,m^3/s}$, and $p_n = 0.88$ Pa).

where n_e gradually decreases and T_e slightly decreases. The values of T_e and n_e in the test region were not considerably different from those observed without the additional

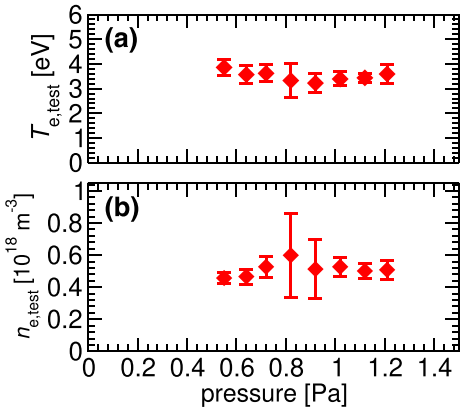

Fig. 9 T_e and n_e in the test region determined using the additional gas feed.

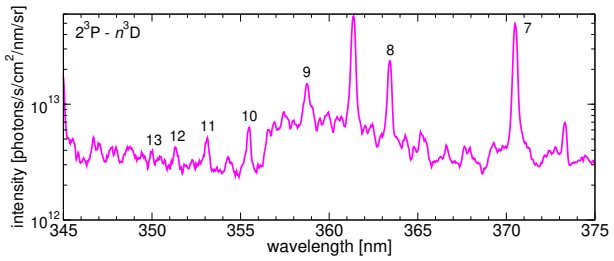

Fig. 10 Spectroscopic data of He obtained using an additional gas feed ($15 \le t \le 55$ ms, $P_{pt} = 4.7$ kW, $Q_p = 0.05$ Pa m^3/s, $Q_t = 0.27$ Pa m^3/s, and $p_n = 0.82$ Pa). The He I, 2^3P–n^3D lines are indicated by the numerals.

feed shown in Fig. 7.

However, different spectra were obtained with and without using the additional feed. That is, $n \le 13$ emissions of HeI 2^3P–n^3D were identified in the spectra obtained using the additional feed, as shown in Fig. 10. However, in experiments with slightly different gas feeding conditions, spectra such as those shown in Fig. 10 could not be clearly identified. In conclusion, there appears to be an extremely narrow range of experimental conditions for generating a recombining plasma.

4.3 Estimation of T_e by the Boltzmann plot method

The electron temperature T_e was estimated by applying the Boltzmann plot method to the observed emissions from the highly excited levels of He. The Boltzmann plot is used to estimate the electron temperature of the recombining plasma from the intensity of high-n line spectra. The observed line spectra of the transition between states of q (low) and p (high) is used to calculate the population density at state p as follows:

$$n_p = \frac{4\pi}{L}\frac{I_{pq}}{A_{pq}}, \tag{2}$$

where I_{pq} is the intensity of the line spectra, A_{pq} is Einstein's A coefficient between the states, and L is the observation length of the plasma. Assuming the local thermal equilibrium (LTE) conditions yields

$$\ln\left(\frac{n_p}{g_p}\right) = -\frac{E_p}{T_e} + \text{const.}, \tag{3}$$

where g_p is degeneracy of the state p, E_p is the energy level of the state p, and T_e is the electron temperature of the plasma. The electron temperature T_e can thus be obtained from the line spectra data. Figure 10 shows the results obtained using the Boltzmann plot. The atomic data used in the calculation are shown in Table 1. Data for the A coefficients were not available for the principal quantum numbers $n \ge 11$ and were estimated by power fitting of $6 \le n \le 10$ data (see Fig. 11).

Table 1 Atomic data of He I.

Transition	E_h [eV]	A_{lh} [s^{-1}]	g_h	Ref.
$2^3P_0 - 7^3D_1$	24.30954	2.1961×10^6	15	[12]
$2^3P_0 - 8^3D_1$	24.37468	1.4479×10^6	15	[12]
$2^3P_0 - 9^3D_1$	24.41933	1.0060×10^6	15	[12]
$2^3P_0 - 10^3D_1$	24.45127	7.2772×10^5	15	[12]
$2^3P_0 - 11^3D_1$	24.47490	$5.2611 \times 10^{5*}$	15	Fig. 11
$2^3P_0 - 12^3D_1$	24.49287	$3.9959 \times 10^{5*}$	15	Fig. 11
$2^3P_0 - 13^3D_1$	24.50686	$3.1025 \times 10^{5*}$	15	Fig. 11

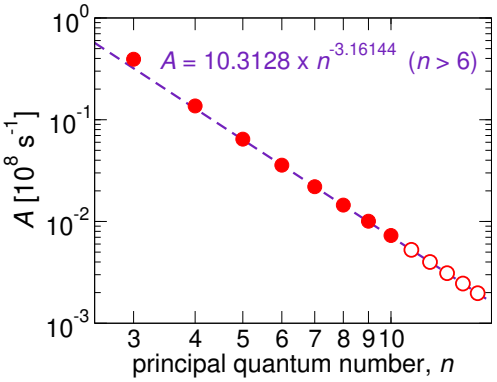

Fig. 11 Power fitting to estimate the A coefficients for $n \ge 11$.

The results are shown in Fig. 12. The plot of the $9 \le n \le 13$ emissions can be approximated by a linear function, which implies that these levels correspond to the LTE. An electron temperature was calculated from these results as T_e of 0.055 eV. This T_e is comparable to those obtained by the same method for other linear plasma devices [13, 14]. Therefore, the volumetric recombination process has been successfully induced in an ECR plasma for the first time, where the observed plasma was under the LTE. The electron temperature evaluated using the Boltzmann plot was significantly different from that measured by the electrostatic probe, $T_e \sim 3$ eV. The probe was placed at 150 mm upstream of the spectroscopic observation point, as shown in Fig. 1. It would be a case that the boundary of the recombining plasma was located between the probe and the spectroscopic observation point. The electron–ion relaxation time τ_{ei} was estimated as follows:

$$\tau_{ei} = \frac{3\sqrt{2}\pi^{3/2}\epsilon_0^2 m_e m_i}{n_i Z_i^2 e^4 \ln\Lambda}\left(\frac{T_e}{m_e}+\frac{T_i}{m_i}\right)^{3/2} \approx 10^{-4}\,\mathrm{s}, \quad (4)$$

where $n_i \sim 10^{18}\,\mathrm{m}^{-3}$ is the ion density, $Z_i = 1$ is the ion charge state, and $\ln\Lambda \sim 20$. This time is comparable with the plasma confinement time t_c in the test region, which was estimated as follows:

$$t_c = \frac{L_p}{C_s} \approx 10^{-4}\,\mathrm{s}, \quad (5)$$

where $L_p \sim 1$ m is the plasma length and $C_s \sim 1.0\times10^4$ m/s is the ion acoustic velocity. Although the two aforementioned time scales are comparable, the actual distance between the probe and spectroscopic observation positions is shorter than the plasma length and the electron temperature decreases by a factor of approximately 1/100 over the actual distance. Therefore, the dramatic temperature change cannot only be explained in terms of the electron–ion relaxation process. There have been reports that a Langmuir probe cannot be used to make accurate recombining plasma measurements because of instantaneous potential fluctuations in the plasma [15–17]. A further analysis of this phenomenon requires detailed measurement of the spatio-temporal distributions of n_e and T_e.

State boundaries lie between different equilibriums. The lower boundary of the energy levels where the LTE is realized is called Byron's boundary p_B [18], and is approximated as follows:

$$p_B \approx \sqrt{\frac{Z^2 R}{3T_e}}, \quad (6)$$

where R is Rydberg's constant in [eV] and $Z = 1$ is the effective nuclear charge. Substituting $T_e = 0.055$ eV results in a value for Byron's boundary of the observed plasma of approximately 9.1. This value is consistent with the fitting range shown in Fig. 12, indicating LTE of the recombining plasma. As the emission intensities obtained from spectroscopic measurements were line-integrated value, the radial profiles of the electron temperature and density need to be measured for further analysis. In a future study, radial measurements will be performed by changing the probe position and the height of the spectroscopic observation point.

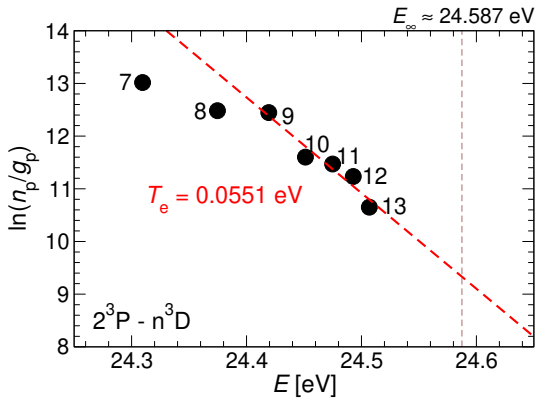

Fig. 12 Boltzmann plot obtained using the intensities of He I, 2^3P–n^3D lines. The vertical line represents the first ionization energy of the helium atom.

4.4 Estimation of n_e using the Saha–Boltzmann equation

The electron density n_e of the recombining plasma can be determined from the Saha–Boltzmann equation based on the result of the Boltzmann plot. At the state p in LTE, the Saha–Boltzmann equation can be written as

$$\frac{n_e n_i}{n_p} = \frac{2g_i}{g_p}\left(\frac{T_e}{4\pi a_0^2 E_{H\infty}}\right)^{\frac{3}{2}} \exp\left(-\frac{E_\infty - E_p}{T_e}\right), \quad (7)$$

where n_i is the density of the He ion, g_i is the degeneracy of the He ion, a_0 is the Bohr radius, $E_{H\infty}$ is the ionization energy of the hydrogen atom, and E_∞ is the first ionization energy of the helium atom. The equation can be transformed by assuming that $p \to \infty$, He^{2+} is absent, the degeneracy of He^+ is $g_i = 2$, and $n_e = n_i$:

$$n_e^2 = 4\frac{n_p}{g_p}\left(\frac{T_e}{4\pi a_0^2 E_{H\infty}}\right)^{\frac{3}{2}}. \quad (8)$$

Substituting $T_e = 0.055$ eV from the Boltzmann plot into Eq. (8) yields the solution as $n_e = 1.33\times10^{18}\,\mathrm{m}^{-3}$. This value is approximately double (and therefore consistent with) that measured by the electrostatic probe. Spectroscopic measurements were simultaneously performed near the end plate in the experiment, but the recombination spectra were not obtained. The locations where recombining plasma was observed were concluded to correspond to that of the recombination front. In future studies, we will measure the spatio-temporal structure of the plasma to facilitate further analysis.

5. Summary

This study was performed to attempt to generate a recombining plasma, which is a prerequisite for forming a detached plasma in NUMBER and carrying out divertor simulation experiments. Experimental difficulties resulted in an insufficient electron density for generating a recombining plasma.

Therefore, the device was modified. A circular polarizer was installed inside the waveguide to convert the linear polarized the incident microwave to a right-handed circular polarized wave. This action reduced the power of the reflected microwave and increased the electron density of the plasma. In particular, the electron density of the plasma increased by a factor of two in the test region. A feed system for a high-flow-rate gas and an additional feed port behind the end plate were installed in the device. This installation enabled the neutral pressure in the test region to be appropriately increased and facilitated conducting experiments using a higher electron density.

An experiment for generating a recombining plasma production was carried out after the modifications. Feeding gas only to the production region increased the electron density, but no characteristic emissions of volumetric recombination, that is, $n \gtrsim 10$ emissions of HeI 2^3P–n^3D, were observed by spectroscopic measurement. However, feeding additional gas feeding to the test region resulted in observation of lines within $n \leq 13$.

The Boltzmann plot method was applied to the observed emission to estimate the electron temperature T_e. The observed emissions were thus determined to be under LTE with $T_e = 0.055\,\mathrm{eV}$, which is comparable to those of other devices that have produced similar plasmas. The first successful induction of volumetric recombination in an ECR plasma was achieved.

The electron density n_e was estimated from obtained T_e by using the Saha–Boltzmann equation. The result was $n_e = 1.33 \times 10^{18}\,\mathrm{m}^{-3}$, which was largely consistent with the electrostatic probe measurement. From these results, it can be concluded that recombining plasma was successfully generated in the NUMBER.

However, it was found that the generation of a recombining plasma could depend on the neutral pressure and flow rate of the fed gas. In a future study, we will further investigate the production conditions. The results of this study constitute a step forward toward performing divertor simulation experiments using NUMBER.

Acknowledgment

This work was supported by JSPS KAKENHI Grant Nos. JP19H01869, JP20H01883 and JP23H01148.

[1] A. Loarte *et al.*, Nucl. Fusion **47**, S203 (2007).
[2] N. Ohno, Plasma Phys. Control. Fusion **59**, 034007 (2017).
[3] N. Ohno *et al.*, Nucl. Fusion **41**, 1055 (2001).
[4] H. Takahashi *et al.*, Plasma Fusion Res. **11**, 2402059 (2016).
[5] D. Hamada *et al.*, Plasma Fusion Res. **13**, 3401044 (2018).
[6] K. Yagasaki *et al.*, J. Nucl. Sci. Technol. (under review).
[7] N. Asakura *et al.*, Processes **10(5)**, 872 (2022).
[8] S. Yoshimura *et al.*, J. Plasma Phys. **81**, 345810204 (2015).
[9] Y. Noguchi *et al.*, Plasma Phys. Control. Fusion **55**, 125005 (2013).
[10] A. Ganguli *et al.*, Phys. Lett. A **250**, 137 (1998).
[11] K. Takahashi *et al.*, Phys. Rev. E **74**, 016405 (2006).
[12] A. Kramida *et al.*, and NIST ASD Team, NIST Atomic Spectra Database (ver 5.10) (2022), online, https://physics.nist.gov/asd [2022, December 22].
[13] D. Nishijima *et al.*, Plasma Phys. Control. Fusion **44**, 597 (2002).
[14] H. Takahashi *et al.*, Trans. Fusion Sci. Technol. **63:1T**, 404 (2013).
[15] N. Ezumi *et al.*, Contrib. Plasma Phys. **38(S1)**, 31 (1998).
[16] N. Ohno *et al.*, Contrib. Plasma Phys. **41(5)**, 473 (2001).
[17] A. Okamoto *et al.*, Contrib. Plasma Phys. **46(5–6)**, 416 (2006).
[18] S. Byron *et al.*, Phys. Rev. Lett. **8**, 376 (1962).